Prevalence and mechanisms of high-level carbapenem antibiotic tolerance in clinical isolates of *Klebsiella pneumoniae*

Trevor Cross[1,2#], Facundo Torres[1,2#], Nadia Nikulin[1,2#], Abigail P. McGee[2*], Leena Jalees[2], Rhea Balakrishnan[2], Tolani Aliyu[2], Lars F. Westblade[3], Abhyudai Singh[4], Tobias Dörr[1,2,5]

[1]Department of Microbiology, Cornell University, Ithaca, NY

[2]Weill Institute for Cell and Molecular Biology, Cornell University, Ithaca, NY

[3] Departments of Pathology and Laboratory Medicine, Medicine, and Pediatrics, Weill Cornell Medicine, New York, NY

[4] Department of Electrical and Computer Engineering, University of Delaware, Newark, DE, 19716, USA

[5] Cornell Institute for Host-Microbe Interactions and Disease (CIHMID)

[*]Current affiliation: Graduate Program in Microbiology and Immunology, Geisel School of Medicine, Dartmouth

[#] these authors contributed equally

Keywords: meropenem, cell envelope stress response, spheroplast, MltB

Abstract:

Antibiotic tolerance is the ability of bacteria to survive normally lethal doses of antibiotics for extended time periods. Clinically significant Enterobacterales, for example, can exhibit high tolerance to the last-resort antibiotic meropenem. Meropenem tolerance is associated with formation of cell wall-deficient spheroplasts that readily recover to rod shape and normal growth upon removal of the antibiotic. Both the true prevalence of tolerance, and genetic mechanisms underlying it, remain poorly understood. Here, we find that meropenem tolerance is widespread among clinical Enterobacterales. Using

forward genetics, we uncover novel tolerance factors in a hypertolerant isolate of the ESKAPE pathogen *Klebsiella pneumoniae*. We find that multiple mechanisms contribute to tolerance, and that cell envelope stress responses (PhoPQ, Cpx, Rcs and OmpR/EnvZ) collectively promote spheroplast stability and recovery, while the lytic transglycosylase MltB counteracts it. Our data indicate that tolerance is widespread among clinical isolates, and that outer membrane maintenance is a key factor promoting survival of tolerant *K. pneumoniae.*

Introduction

Healthcare-associated infections are common sequelae of hospitalization. Increasingly, treatment of these infections fails due to antibiotic resistance [1]. However, treatment also often fails despite the absence of outright resistance [2]. This has been attributed to other bacterial strategies for evading complete eradication, including the well-characterized phenomenon of bacterial persistence [3]. However, between the extremes of frank resistance and persistence, there is considerable complexity in bacterial antibiotic susceptibility patterns. For example, antibiotic tolerance, which has recently received increased attention as another means of surviving antibiotic insult, represents a state where a large fraction of susceptible bacteria survives in the presence of an antibiotic for extended periods. Gram-negative bacteria in particular can enter a non-replicative, cell wall-deficient spheroplast form upon treatment with β-lactam antibiotics [4-7]. This phenotype is reminiscent of L-forms [8-10] with the distinction that spheroplasts (unlike L-forms) do not proliferate in the presence of antibiotic. Spheroplasts remain intact for extended time periods and readily recover their cell shape and resume division when the

48 β-lactam drug is removed. While tolerant spheroplasts have been characterized in diverse
49 Gram-negative pathogens [5-7], the true prevalence of β-lactam tolerance among Gram-
50 negative clinical isolates is unknown.

51 *Klebsiella pneumoniae* is a Gram-negative nosocomial pathogen that can cause a
52 variety of opportunistic infections, including eponymous pneumonia, bloodstream
53 infections and UTIs [11]. A member of the infamous ESKAPE group of pathogens, *K.*
54 *pneumoniae* exhibits particularly worrisome levels of treatment failure [12]. Due to the
55 high level of resistance against most β-lactams, the carbapenems remain one of the
56 leading antibiotic classes that are still effective against *K. pneumoniae* [13]. Determining
57 mechanisms that alter susceptibility against β-lactams in general, and carbapenems in
58 particular, is thus a critical need for developing new treatment options against *K.*
59 *pneumoniae.* β-lactams covalently and irreversibly bind to so-called penicillin-binding
60 proteins (PBPs), which are the principal synthases of the main cell wall component
61 peptidoglycan (PG). β-lactam binding results in several downstream events that
62 contribute to cell death in poorly-defined ways [14]. Endogenous cell wall lytic enzymes
63 (collectively referred to as autolysins) degrade PG into monomers and ultimately eliminate
64 the sacculus entirely. In some bacteria, cell wall degradation can cause catastrophic
65 rupture and cell lysis, for example in the well-studied model organism *E. coli.* In addition,
66 the constant synthesis and immediate autolysin-mediated degradation of PG (futile
67 cycling) depletes cellular resources, potentially exacerbating detrimental effects
68 independent of cell lysis [15, 16]. Interestingly, β-lactam exposure coincides with the
69 generation of damaging reactive oxygen species (ROS), though the contribution of ROS
70 to β-lactam killing is not entirely clear [17]. It is thought that the combination of these

71 direct and indirect effects collectively contributes to cell death by lysis and/or internal
72 damage. How tolerant cells manage this assault to stay alive has remained poorly
73 understood, but previous work has implicated cell envelope stress signaling in
74 spheroplast survival [17-19]. In the cholera pathogen *Vibrio cholerae*, for example, the
75 VxrAB system is induced by β-lactam stress, resulting in the upregulation of cell wall
76 synthesis functions (which likely readies the cell for recovery once the antibiotic is
77 removed) and downregulation of detrimental iron influx (putatively to reduce the damage
78 sustained by ROS production) [17].

79 In this study, we sought to characterize meropenem tolerance in *K. pneumoniae*. We
80 found that clinical isolates of this nosocomial Gram-negative pathogen often exhibit high
81 levels of meropenem tolerance. Using TnSeq, we defined genetic requirements for
82 tolerance, and uncovered a role for cell envelope stress signaling systems in both
83 spheroplast maintenance and recovery. Our data open the door for a more in-depth
84 understanding of the molecular mechanisms promoting tolerance, priming the future
85 design of antibiotic adjuvants that eradicate tolerant cells.

86

87 **Results**

88 *Klebsiella species clinical isolates exhibit high meropenem tolerance*

89 As part of a larger effort to determine the role of antibiotic tolerance in healthcare settings,
90 we characterized a large panel of bloodstream isolates from the culture collection of Weill
91 Cornell Medicine (WCM). This de-identified 271 isolate panel (**Table S1, S3**) has been
92 fully characterized through antimicrobial susceptibility testing and consists of Gram-

93 negative pathogens that are mostly carbapenem-susceptible (MIC <1 μg/mL), with three
94 isolates testing as intermediate (MIC = 2) and seven strains as fully resistant (MIC > 4
95 μg/mL; one strain due to its possession of a KPC carbapenemase). Specifically, the panel
96 consists of 52 % *Escherichia coli* isolates, 30 % *Klebsiella pneumoniae*, 9 %
97 *Pseudomonas aeruginosa*, 6 % *Enterobacter cloacae* complex, 2 % *Klebsiella variicola*
98 and 1 % *Acinetobacter baumannii* complex. Since the majority of the isolates are
99 carbapenem susceptible, we considered this an ideal panel for determination of how
100 prevalent carbapenem tolerance (rather than resistance) is in clinical samples. Currently,
101 no fully-established sufficiently high throughput tolerance assay exists (we considered
102 another established tolerance test, the TDtest [20] as less effective for our purposes due
103 to the high number of plates required), and we therefore chose to use a semi-quantitative
104 assay for our screen. To this end, we grew the isolate panel (curated to remove the
105 resistant isolates with MIC > 4 μg/mL with the exception of the KPC producer as an
106 example of full resistance) in a 96-well format, where we exposed cells to meropenem
107 (10 μg/mL, 5x – 100x MIC) at high cell densities (following a 10-fold dilution of overnight
108 culture into fresh medium) in Brain-Heart Infusion broth. At the 8 hour and 24 hour
109 timepoints, 5 μL of thus-treated cultures were then spotted on an agar plate together with
110 5 ng of purified carbapenemase (KPC-2) to remove the antibiotic. After 24 hours of
111 incubation, spots were then scored as full growth (a confluent spot = high tolerance),
112 growth with a few visible colonies (= intermediate) or no growth (= low tolerance) (**Fig.
113 1A, Table S1**). Since this panel contained isolates exhibiting a wide distribution of
114 susceptibilities to meropenem (MICs ranging from ≤0.015 – 4 μg/mL), we considered the
115 possibility that apparent differences in tolerance may instead reflect differences in MIC.

116 Plotting tolerance categories over MIC values revealed that all 3 tolerance categories
117 contained isolates with similar variance in MICs (**Fig. 1B**). As an example, all isolates in
118 **Fig. 1A** with a yellow circle had comparatively high MICs (>/= 1 μg/mL), but displayed
119 very different survival levels at 8 and 24 hours of meropenem exposure. While we did
120 observe a slight and statistically significant positive correlation between tolerance
121 category and MIC (**Fig. 1B),** the large overlap in MIC between categories and the
122 weakness of the correlation (Spearman coefficient $\rho = 0.22$, $p = 3.72^{-4}$) suggest an
123 insignificant relationship between tolerance and intrinsic resistance. Thus, tolerance as
124 determined in this assay is not a simple function of MIC variation; rather, these data
125 suggest that our assay largely captures true tolerance.

126

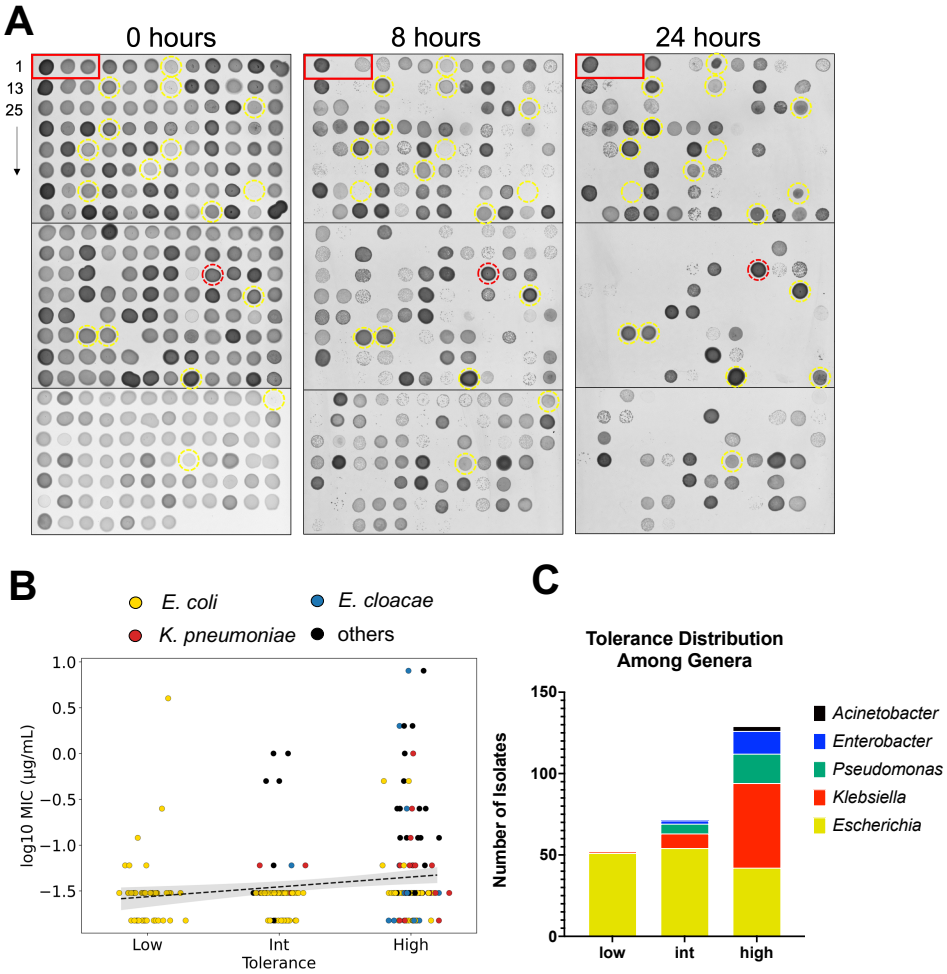

Figure 1: Widespread meropenem tolerance among bloodstream isolates

(A) A panel of susceptible bloodstream isolates (meropenem MIC </= 4 µg/mL, n=263, see text for details) was exposed to 10 µg/mL (>2x MIC for all isolates) meropenem in 96-well format (BHI medium) and incubated for 8 hours or 24 hours. Following incubation, purified KPC-2 enzyme was added to the wells, and 10 µL transferred to a BHI plate without antibiotic. Tolerance was scored qualitatively as the ability to form colonies/confluent growth after 8 or 24 hours. Yellow circles indicate examples of different tolerance levels across high MIC (>/=1 µg/mL). Red circle indicates a positive control isolate (resistant, KPC+). Red box indicates examples of (from left to right) a highly tolerant *Klebsiella pneumoniae* isolate, an intermediate tolerant *E. coli* and a low tolerant *E. coli.* (B) Tolerance categories were plotted with their corresponding MIC values). Black line indicates weak correlation between tolerance and MIC (Spearman's coefficient = 0.22) (grey area represents 95% confidence interval). Raw data are color-coded according to species (C) Genus distribution among the tolerance categories.

143 We then asked whether some genera were more likely to exhibit tolerance than
144 others, and to this end plotted tolerance as a function of bacterial genus. Interestingly, the
145 low tolerance fraction was almost exclusively occupied by *E. coli* isolates (consistent with
146 our previous observations [7]), while in the high tolerance fraction, *Enterobacter species.,*
147 *Pseudomonas aeruginosa*, and especially *Klebsiella pneumoniae* were highly
148 represented (**Fig. 1C, Table S1**). Statistical analysis confirmed a strong enrichment for
149 *E. coli* in the low tolerance category (odds ratio = 59.94, $p = 5.2x10^{-13}$), and enrichment
150 for *K. pneumoniae* in the high tolerance category (odds ratio = 7.18, $p = 8.4x10^{-9}$). Thus,
151 *K. pneumoniae* clinical isolates in this panel are more likely to display antibiotic tolerance
152 compared to *E. coli*.

153

154 *The K. pneumoniae TS1 isolate is highly meropenem tolerant*

155 Since *K. pneumoniae* clinical isolates answered our survey as particularly tolerant,
156 we chose to focus on this species for further study of meropenem tolerance. However,
157 we noted that different *K. pneumoniae* isolates diverged in tolerance levels in our spot
158 assay (**Fig. 1A**). To more quantitatively determine strain-specific differences, and to
159 identify new model strains for mechanistic studies, we compared two well-characterized
160 clinical isolates of *K. pneumoniae* for their tolerance levels *in vitro*, namely *K. pneumoniae*
161 strains TS1 (a derivative of the CDC isolate bank AR0080) and KPNIH1 [21]. Both strains
162 have been cured of their carbapenemase-containing plasmids and are thus fully
163 meropenem susceptible with MIC's of 0.05 (KPNIH1) and 0.1 (TS1), respectively (**Table**
164 **S2**). Time-dependent killing experiments in the presence of 10 μg/mL meropenem

165 revealed substantial differences in tolerance levels between the two strains, despite their

166 similar susceptibility (**Fig. 2, Table S2**).

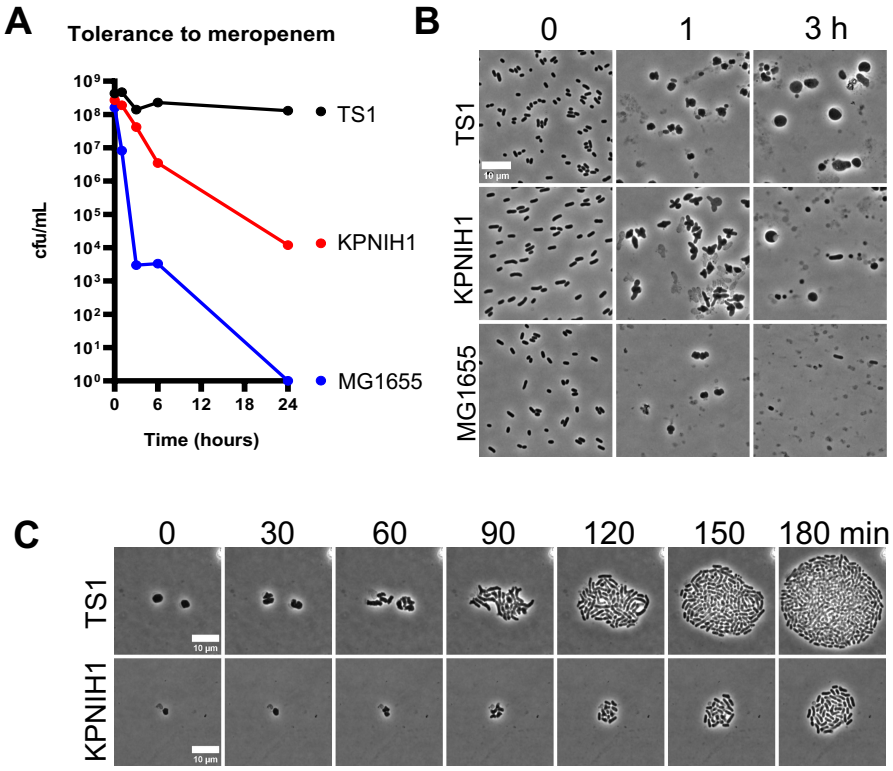

167

168 **Figure 2: *K. pneumoniae* TS1 is a hypertolerant clinical isolate**

169 (A) Example time-dependent killing experiment (BHI medium) in meropenem (10 µg/mL)
170 reveals differences in tolerance levels among two *K. pneumoniae* isolates (with the model
171 *E. coli* strain MG1655 as comparison). (B) Tolerance in *K. pneumoniae* is associated with
172 spheroplast formation. Aliquots from the experiment depicted in panel (A) were
173 transferred to agarose slides at the indicated time-points and imaged. (C) Recovery after
174 addition of purified KPC-2 carbapenemase demonstrates spheroplast viability. Scale bar
175 = 10 µm.

176

177 This observation supports our previous finding of often different tolerance levels

178 between different isolates of the same species [7]. Both *K. pneumoniae* strains still

179 exhibited higher levels of survival relative to the low-tolerance *E. coli* MG1655 comparison

180 strain, which exhibited a steep, 4.5 log reduction in viability within six hours of meropenem
181 treatment, and complete elimination by 24 hours of exposure. The TS1 strain was almost
182 completely tolerant, with only a slight (5-10 fold) decrease in viability even after 24 hours
183 of exposure (**Fig. 2A**). In contrast, the KPNIH1 isolate lost viability by 10,000-fold after 24
184 hours. In *both Klebsiella* isolates, survival coincided with formation of cell wall-deficient
185 spheroplasts (**Fig. 2B**) that readily recovered to rod-shape morphology upon removal of
186 the antibiotic (**Fig. 2C**). We also used these three benchmark strains to validate our high-
187 tolerance spot assay (**Fig. S1**). Consistent with the time-dependent killing experiments
188 (**Fig. 2A**), TS1 scored as highly tolerant, KPNIH1 as intermediate, and MG1655 as non-
189 tolerant in the spot assay (**Fig. S1**). Thus, the TS1 isolate is highly meropenem tolerant,
190 and serves as an ideal model for a mechanistic characterization of spheroplast formation
191 and recovery.

192

193 *A TnSeq approach reveals putative tolerance genes in K. pneumoniae* TS1

194 We next sought to identify factors that contribute to meropenem tolerance in *K.*
195 *pneumoniae*. To this end, we conducted a transposon-insertion sequencing screen to
196 assemble a genome-wide mutant fitness map in the presence of meropenem and
197 compared insertion frequencies before and after 6 hours of meropenem exposure
198 (including an outgrowth step, see methods for details, **Fig. 3A**).

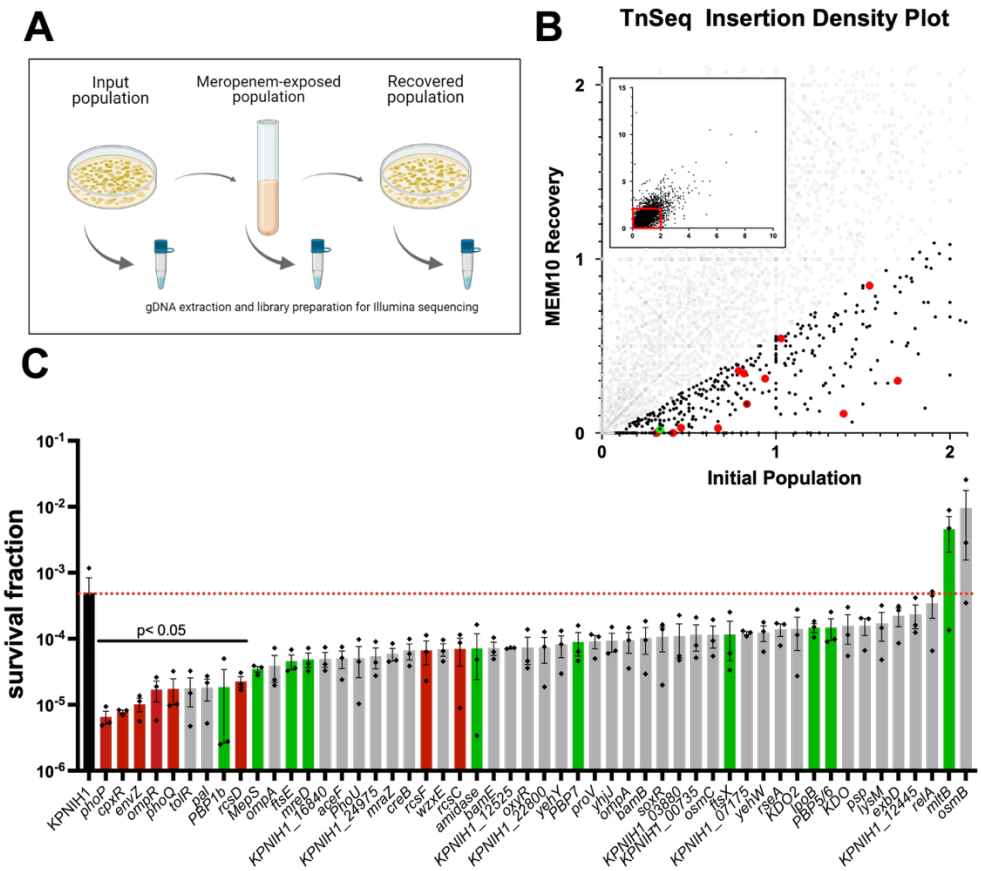

Figure 3: TnSeq identifies genetic determinants of meropenem tolerance.

(A) Outline of TnSeq experimental procedure. (B) Identification of candidate tolerance factors in TS1 by plotting insertion density of a recovered library vs. the input library. Shown is a scatterplot of Tn insertion frequencies before (x-axis) vs. after (y-axis) meropenem exposure (inset indicates all genes, main panel represents a zoomed version of the red box in the inset). *Bona fide* tolerance genes are those that have a lower insertion frequency after exposure vs. pre-exposure. Red and green dots represent examples of tolerance genes prioritized for further validation (C) Validation of TnSeq hits. Mutants were obtained from the KPNIH1 mutant library and exposed to meropenem (10 µg/mL) for 6 hours, followed by dilution and spot-plating. Raw data of 3 independent biological replicates are shown +/- standard deviation. Red dotted line indicates WT average survival level. Red bars indicate cell envelope stress response systems; green bars represent genes involved in cell wall homeostasis. Statistical significance was established via Kruskal-Wallace test comparing each mutant to WT.

The screen uncovered both expected and novel putative tolerance genes (**Fig. 3B, Table S4**). Notably, the gene coding for PBP1b was detected within the top two percent

217 of candidate essential genes for tolerance to meropenem. Class aPBPs like aPBP1b have
218 an established role in rebuilding the cell wall after damage [22, 23], and thus serve as
219 internal validation of our screening conditions, establishing confidence in our TnSeq
220 approach. Next, we validated our most prominent hits (i.e., those with the highest insertion
221 rate pre- vs post-exposure). We used an ordered, commercially available transposon
222 insertion library in the intermediate tolerance strain KPNIH1 [21] for a first-pass validation.
223 This resulted in confirmation of several genes whose inactivation either promoted or
224 reduced tolerance (**Fig. 3C**). The reduced tolerance fraction contained cell envelope
225 functions, albeit some without statistical significance, due to the high variance in this pilot
226 screening assay (**Fig. 3C**, green bars). An involvement of cell envelope functions is
227 expected due to the need to re-establish a cell wall upon spheroplast recovery. We also
228 noticed that disruptions in several cell envelope stress response systems (*rcs*, *pho*, *cpx*,
229 and *ompR-envZ*), drastically and statistically significantly reduced survival during
230 meropenem stress (**Fig. 3C**, red bars), while two gene disruptions (in the gene for the cell
231 wall lytic enzyme MltB, and in the poorly characterized outer membrane lipoprotein
232 OsmB), increased survival. Taken together, these results demonstrate that the *K.*
233 *pneumoniae* TnSeq experiment was effective at identifying specific genes with roles in
234 meropenem tolerance, lending themselves to further study as outlined below.

235

236 *The lytic transglycosylase* MltB *endogenously reduces meropenem tolerance*

237 Our TnSeq screen identified both genes that promote meropenem tolerance as
238 well as genes whose products are actually detrimental in the presence of antibiotic.
239 Inactivation of the gene coding for the lytic transglycosylase enzyme MltB, for example,

240 answered the screen as imparting a fitness advantage in the presence of meropenem,
241 suggesting that MltB plays a role in meropenem-mediated killing. The specific phenotype
242 for MltB was unexpected, since bacteria generally have many functionally redundant lytic
243 transglycosylase paralogs throughout their genomes, and phenotypes associated with a
244 single deletion are thus rare [24]. To dissect the role of LTGs in meropenem tolerance
245 further, we tested a panel of transposon disruption mutants in known and predicted LTG
246 genes for meropenem tolerance in the lower tolerance strain KPNIH1. Among eleven
247 mutants tested, only *mltB::tn* and (to a lesser degree) *sltY::tn* exhibited significantly
248 increased survival in the presence of meropenem, with a drastic 1000-fold increase in
249 survival (compared to WT) after 24 hours for *mltB* and 100-fold for *sltY* (**Fig. 4A**). Time-
250 dependent killing experiments confirmed a strong role for MltB as an antagonist of
251 antibiotic tolerance, as the *mltB::tn* mutant exhibited minimal (5-fold) killing in the
252 presence of meropenem over 24 hours (**Fig. 4B**); this phenotype could be complemented
253 by expressing inducible *mltB* from a neutral chromosomal locus (**Fig. S2**).

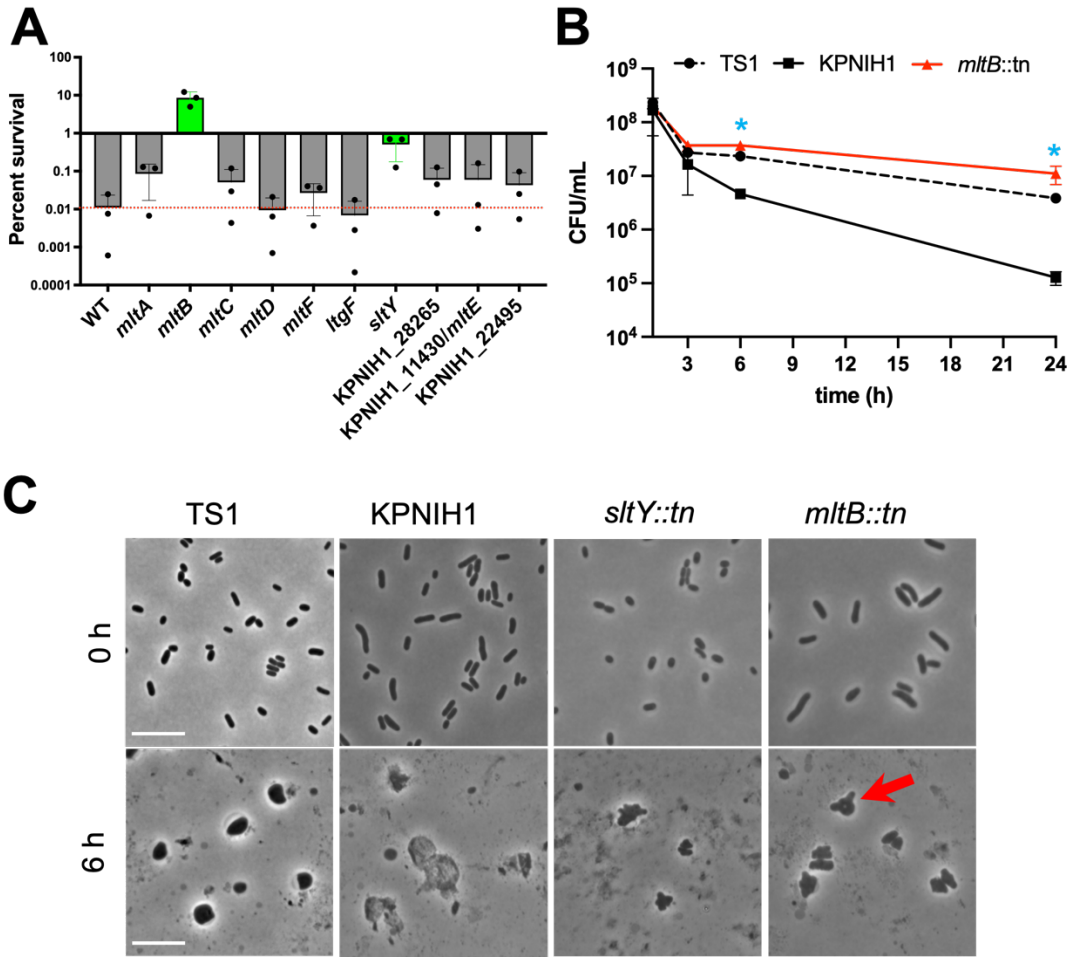

Figure 4: MltB and SltY reduce tolerance to meropenem and prevent cells from retaining polar morphology

(A) Survival of mutants in lytic transglycosylases. Mutants were obtained from the KPNIH1 mutant library and exposed to meropenem (10 µg/mL) for 6 hours, followed by dilution and spot-plating. (B) Time-dependent killing reveals increased tolerance in an *mltB* mutant. Shown are mean +/- SD of 6 biological replicates for *mltB::tn* (3 replicates for both WT) * = $p < 0.05$, Mann Whitney test. (C) Cell wall degradation in LTG mutants. Bacteria were treated as described for A and then imaged at the indicated timepoints. Red arrow points to an example of a retained pole in *mltB::tn.* The hypertolerant TS1 strain is shown as comparison. Scale bars, 10 µm.

The *mltB::tn* and *sltY:tn* mutants were further characterized by examining cell morphology upon spheroplast formation. Timelapse microscopy of cells exposed to meropenem revealed that the *mltB::tn* and *sltY:tn* disruption mutants were clearly

damaged by the antibiotic (forming spheroplasts). However, *mltB::tn* retained morphology at the cell poles for longer than the parent strain (**Fig. 4C**, red arrow), and qualitatively exhibited an increase in the relative abundance of intact spheroplasts (**Fig. 4C**). These data suggest that *mltB* and (to a lesser extent) *sltY* may reduce tolerance by accelerating the degradation of peptidoglycan when synthesis is halted by meropenem, and thus point to a dominant role of these LTGs in cell wall turnover in *K. pneumoniae*. Perhaps activation of autolysins could be a useful future strategy to potentiate β-lactam antibiotics against tolerant pathogens.

Multiple cell envelope stress response systems collectively contribute to β-lactam tolerance

Several well-characterized cell envelope stress response systems appeared in our screen as top candidates that promote meropenem tolerance: the Rcs phosphorelay system, the PhoPQ and CpxAR two-component systems, and the osmotic and acid stress response TCS, OmpR/EnvZ. Of note, our previous work revealed the PhoPQ system as a key meropenem tolerance determinant in the fellow Enterobacterales, *Enterobacter cloacae,* suggesting that PhoPQ-mediated tolerance may be a widely conserved [25]. To dissect the individual and combined contributions of these systems to survival in meropenem, we created deletions of all four systems in all combinations, including one quadruple system deletion mutant lacking all four stress responses, in our hypertolerant TS1 strain. These mutants were then exposed to meropenem in time-dependent killing assays. These experiments revealed a 10 to 10,000-fold decrease in viability after 24 hours of exposure to meropenem in any individual envelope stress response mutant

compared to the wild type *K. pneumoniae* parent strain (**Fig. 5AB**), which could be complemented by expressing each respective system from a neutral chromosomal locus (**Fig. S4**). We observed large differences in both magnitude and consequences for lysis in the different mutants. The Δ*ompR/envZ* mutant, for example, exhibited the most drastic reduction in viability of all the single mutants (10,000-fold vs. 10- to 100-fold for the others), pointing to a particularly important role of the OmpR/EnvZ response in tolerance to meropenem. We also noticed that while most single mutants exhibited both a drop in CFU/mL and in OD_{600} (indicative of cell lysis), the Δ*rcsF* mutant was only defective in viability, with only a slight reduction in OD during meropenem treatment (**Fig. 5A**), suggesting a role for RcsF in spheroplast recovery, rather than structural maintenance.

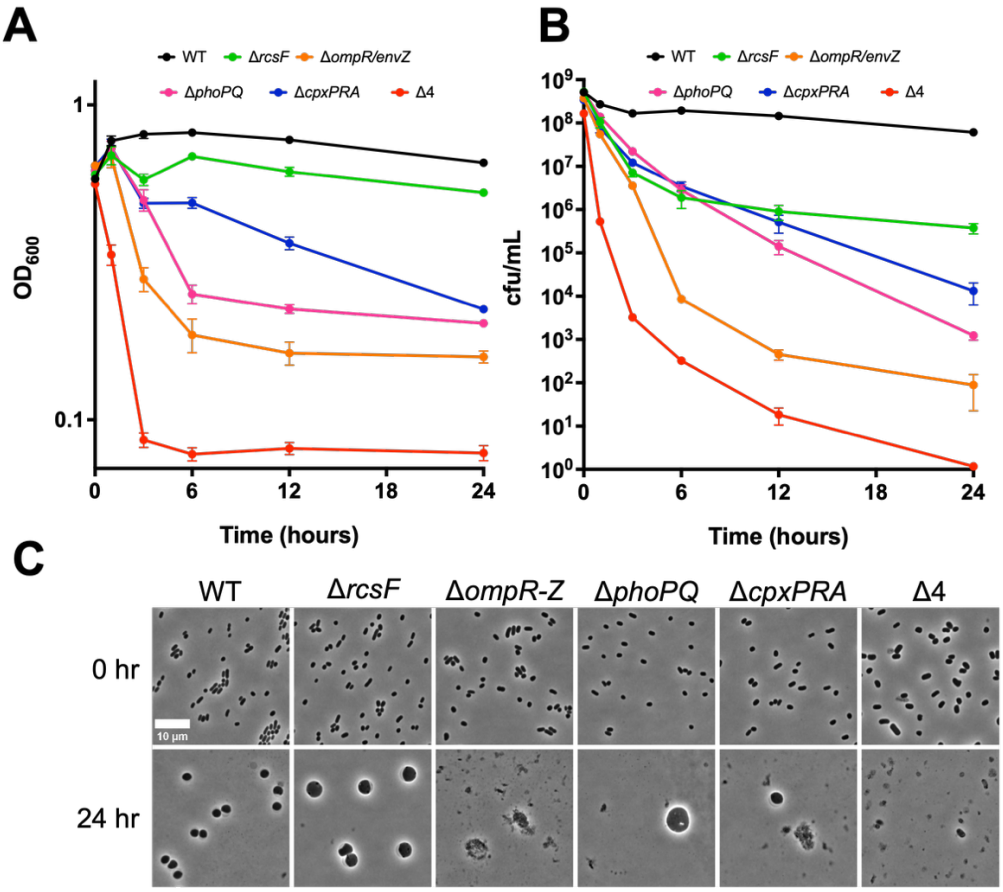

303 **Figure 5: Cell envelope stress response systems are essential for full meropenem**
304 **tolerance**

305 TS1 and its mutant derivatives were diluted 10fold into 5 mL of BHI medium containing
306 10 µg/mL meropenem. At the indicated timepoints, samples were withdrawn and OD_{600}
307 (A) and CFU/mL (B) were measured. At 24 hours, differences between each mutant and
308 WT, and between ∆4 and each single mutant except ∆*ompR*/*envZ* were statistically
309 significant (Mann Whitney U test, p = 0.002). mutant (C) Aliquots were removed from the
310 experiment depicted in (A-B) and imaged. Scale bar = 10 µm.

311

312 We also investigated cell morphologies of each mutant before and after exposure
313 to meropenem for 24 hours of treatment, and upon recovery in strains capable of forming
314 spheroplasts. Wild type cells and all single deletion mutants appeared similar in shape
315 and morphology at the start of meropenem exposure experiments (**Fig. 5C**). However,
316 the Δ4 mutant cells exhibited slightly aberrant morphology (slightly larger cells with subtle
317 deformations) and spontaneous lysis, suggested by the presence of cell debris. After 24
318 hours of meropenem exposure, CESR single deletion mutants formed spheroplasts,
319 albeit at much lower numbers compared to WT. The exceptions to this were the
320 Δ*ompR/envZ* mutant, in which spheroplasts were not observed, and the *rcsF* mutant,
321 which formed robust spheroplasts, consistent with the relatively minor reduction in OD_{600}
322 post-treatment (**Fig. 5C**). Thus, the Rcs system may play a role in spheroplast recovery,
323 rather than spheroplast cell envelope maintenance, consistent with a role in spheroplast
324 recovery in lysozyme-treated *E. coli* [26]. Interestingly, the Δ*ompR/envZ* and Δ4 mutants
325 were highly defective in spheroplast formation or maintenance, as we failed to find any
326 intact spheroplasts even upon 10-fold concentration of meropenem-treated culture
327 followed by imaging, consistent with the drastic reduction in viability these strains
328 experience in the presence of meropenem (**Fig. 5B**). We also constructed intermediate
329 strains, including a suite of ∆3s with single two-component systems left intact (**Fig. S3**).

330 All Δ3s collapsed in viability almost to the same degree as the Δ4, strongly suggesting an
331 additive or synergistic effect between the different systems, as no two-component system
332 by itself could sustain viability. Of note, among the Δ2 mutants, the combination of
333 Δ*ompR/envZ* and Δ*rcsF* was most detrimental, and the resulting mutant was, like the Δ4
334 mutant, nearly eradicated after 24 hours of exposure. Collectively, these results point to
335 a functionally hierarchical organization of responses necessary for meropenem tolerance:
336 OmpR/EnvZ as the most important response, followed by Pho and Cpx to maintain
337 spheroplast stability, and Rcs with a more prominent role in recovery compared to
338 maintenance of structural integrity.

339

340 *The Rcs phosphorelay is induced by, and required for, meropenem tolerance*

341 The Rcs phosphorelay as an apparent contributor to tolerance caught our attention. In *E.*
342 *coli*, Rcs is induced by β-lactams, and required for survival in low β-lactam concentrations
343 [27]. Additionally, Rcs is required for recovery of *E. coli* from a cell wall-deficient state
344 (generated by lysozyme treatment in osmostabilized medium, a condition that
345 morphologically mimics meropenem-treated spheroplasts) [26]. In apparent contrast, a
346 recent study has shown that Rcs is neither induced by, nor required for β-lactam
347 persisters [28]; however, this is likely because persisters are dormant and thus not
348 expected to be damaged by the antibiotic (obviating the need for a damage response) [3].
349 To clarify the role of Rcs in *K. pneumoniae*, we engineered a TS1 strain carrying an P_{rprA}-
350 *lacZ* transcriptional fusion (a well-established readout of Rcs signaling [29]) in a neutral
351 chromosomal locus (*lacZ*) and measured induction by meropenem. A first qualitative
352 assay using zone of inhibition on growth medium containing the chromogenic LacZ

substrate X-gal yielded a blue ring around the zone of inhibition when a meropenem disk was placed on the agar surface, but not when the translation inhibitor kanamycin was used (**Fig. S5A**). We then corroborated these results in liquid medium, where a quantitative β-galactosidase activity assay (Miller assay) revealed a 5-fold induction of the construct by meropenem that was largely dependent on the presence of RcsB (**Fig. 6A**). Thus, meropenem induces the Rcs response. We also validated the role of Rcs in meropenem tolerance by creating additional mutants in Rcs components, namely RcsC and RcsD. All mutants displayed a strong (10,000fold) reduction in tolerance, which could be fully complemented by overexpression of the response regulator RcsB (**Fig. 6B**). The ability of RcsB overexpression to induce the Rcs regulon was verified by measuring induction of the chromosomal P_{rprA}-*lacZ* construct (**Fig. S5B**). Thus, the Rcs phosphorelay is both responsive to meropenem exposure, and required for meropenem tolerance in *K. pneumoniae.*

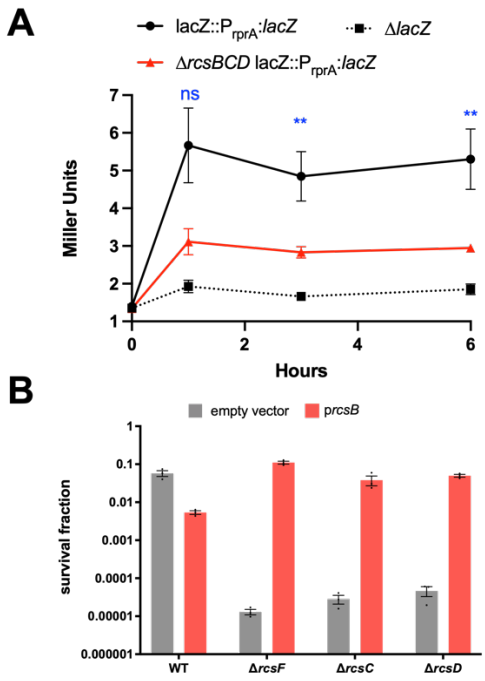

367 **Figure 6: The Rcs phosphorelay is induced by meropenem and required for**
368 **tolerance**

369 (A) WT and Δ*rcsBCD* strains carrying a chromosomal rprA-*lacZ* transcriptional fusion
370 were exposed to meropenem, followed by quantification of beta-galactosidase activity via
371 Miller assay. A strain deleted in *lacZ* was used as background control. ** = $p<0.05$, ns =
372 not significant (t-test) (B) The indicated strains were exposed to meropenem (10 µg/mL).
373 Survival fraction is CFU/mL after 24 hours normalized to starting cell density. Shown are
374 averages of 3 independent experiments +/- standard error.

375

376 *Fluctuation test reveals memory in tolerant subpopulation*

377 The stress responses that contribute to meropenem tolerance may rely on deterministic
378 induction by the antibiotic for their protective impact, or they may be stochastically and
379 heterogeneously active within the population before exposure to a stress as a bet-hedging
380 strategy. To gain some insight into this distinction, we leveraged the classical Luria-
381 Delbrück experiment or the "Fluctuation Test" that has been recently expanded to
382 investigate reversible switching between cellular states within an isogenic cell population.
383 This fluctuation test has been used to gain insights into the non-genetic mechanisms by
384 which microbial and cancer cells survive lethal exposure to targeted drug therapy [30-32].
385 For example, the application of the fluctuation test in both *Escherichia coli* [33], *Bacillus*
386 *megaterium* [34] and *Mycobacterium tuberculosis* [35] has shown individual cells to
387 reversibly switch between an antibiotic-sensitive and an antibiotic-tolerant state, with each
388 state being maintained transiently for several generations. This reversible switching
389 happens continuously in the absence of the drug as a result of stochastic fluctuations in
390 underlying signaling and gene regulatory networks and primes a rare subpopulation of
391 cells as a bet-hedging mechanism to survive lethal antibiotic exposure.

392 To conduct a fluctuation test, we first isolated single TS1 cells in 96-well plates
393 using serial dilution. Each cell was grown into a clonal population and exposed to
394 meropenem at an OD_{600} of 0.3 (**Fig. 7**). WT OD dropped sharply at first, followed by
395 slower increase in OD_{600} in the surviving subpopulation (spheroplasts). The clone-to-
396 clone fluctuations in cell viability after antibiotic exposure were quantified by using the
397 coefficient of variation (standard deviation divided by the mean) of OD_{600} (spheroplast
398 survivor fraction) across clones at 1.66 hours after drug exposure. This time point was
399 specifically chosen as it captures the OD_{600} drop-off in response to meropenem (**Fig. 7,**
400 dashed vertical red line) and avoids the rebound in OD_{600} seen in WT cells as a result of
401 changes in cell shape. We then used mathematical modeling to predict how the kinetics
402 of switching between drug-sensitive and drug-tolerant cell states impact clone-to-clone
403 fluctuations in the number of cells surviving lethal stress, with slower switching (i.e., higher
404 transient memory of a state being retained across generation) resulting in a higher degree
405 of interconal fluctuations [32]. Our results show clone-to-clone fluctuations in cell integrity
406 to be 0.153 ± 0.036 for WT where $\pm$ denotes the 95% confidence intervals in the
407 coefficient of variation of OD_{600} as obtained by bootstrapping (**Fig. 7**). These observed
408 fluctuations were significantly higher than the technical noise of 0.086 ± 0.028 (control
409 fluctuations). Technical noise was estimated by performing a similar experiment, but with
410 fluctuations quantified across wells starting with a random population of 10,000 cells
411 rather than a single cell-derived population. These results were statistically significant
412 (testing for equality of CVs [36]; $p = 0.0031$ for WT 1 cell vs. 10^4 cells; $p = 9.7 \times 10^{-6}$ for
413 $\Delta 4$ one cell vs. 10^4 cells). Similar to observations in other bacteria, this fluctuation data is

414 consistent with a model of a multi-generation drug-tolerant state in *Klebsiella pneumoniae*

415 that preexists meropenem exposure.

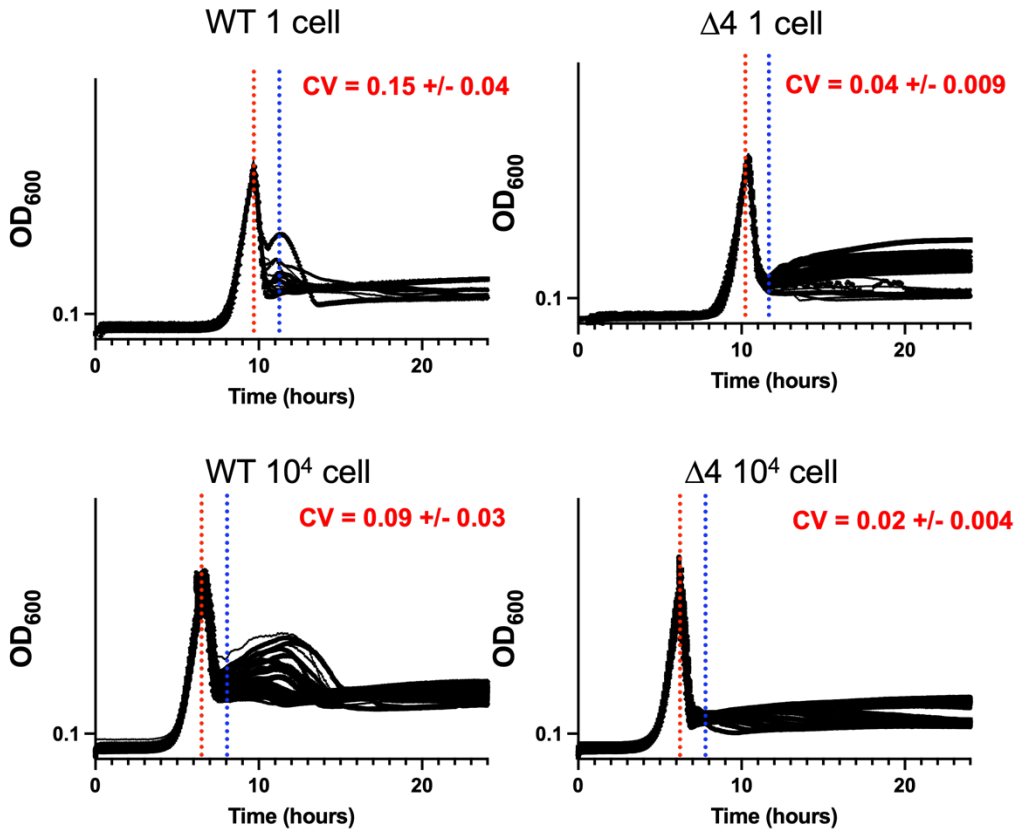

416

417 **Figure 7. Fluctuation test indicates memory in spheroplast population.** Bacteria
418 were diluted to a starting density of 1 cell/well or 10,000 cells/well (control), and grown
419 in a microtiter plate. At OD_{600} =0.3, meropenem (10 µg/mL) was added (red dotted line).
420 CV (coefficient of variation) calculations were performed at peak killing (blue dotted
421 line).

422

423 We hypothesized that the stochasticity originated from variance in background expression

424 of cell envelope stress responses. To test this, we repeated the fluctuation assay in the

425 Δ4 genotype where the observed fluctuations were much smaller compared to WT with

426 the coefficient of variation being 0.044±0.009, but still significant compared to control

427 fluctuations performed for this strain (**Fig. 7**). The lower value of the observed clonal

428 fluctuations in Δ4 points to faster-switching kinetics, and hence a shorter transient
429 memory of the drug-tolerant state.

430 **Discussion**

431 Infections with Enterobacterales continue to be an active and increasing threat to
432 public health due to their capacity to cause infection, and to gain and disseminate
433 antibiotic resistance genes, with particular risk for vulnerable populations. In this work, we
434 have found that antibiotic tolerance, the ability to sustain viability in the presence of
435 bactericidal antibiotics for extended time periods, is widespread among clinical isolates
436 of Gram-negative pathogens, particularly *Klebsiella pneumoniae*.

437 To uncover novel factors that modulate β-lactam tolerance in *K. pneumoniae* we
438 performed a genome-wide scan using a TnSeq approach. Because this approach
439 provides a readout of each gene's fitness during a challenge, we were able to identify
440 genes that contribute to meropenem tolerance, and genes that reduce tolerance in *K.*
441 *pneumoniae*. The screen overall was able to capture several regulatory systems and
442 individual factors that modulate tolerance along with the internal control PBP1b (a key
443 cell wall synthase required to rebuild the cell wall after catastrophic damage [23]), raising
444 confidence in our approach. This screen also pointed to several cell envelope stress
445 responses that are partly responsible for this strain's ability to undergo the entire process
446 of spheroplast formation, maintenance, and recovery: the Rcs, Pho, Cpx, and
447 OmpR/EnvZ systems. Of note, the ability of cell envelope stress responses to confer
448 antibiotic tolerance via repair of antibiotic-induced damage appears to be widespread
449 among diverse bacteria [14, 17, 37, 38].

450 Interestingly, the OmpR/EnvZ system appears to exert a particularly strong effect
451 on tolerance. This system is induced by changes in pH and osmolarity, and in *E. coli*
452 controls the switch from the larger diameter porin OmpF to the smaller diameter porin
453 OmpC [39]. Formally, it is possible that the porin switch may delay diffusion of meropenem
454 into the cell; however, this is unlikely to account for the tolerance phenotype we observe
455 here, given that WT and Δ*ompR/envZ* MICs are within essential agreement (**Table S2**).
456 Future work will be directed at delineating the contribution of this system to spheroplast
457 maintenance. Conversely, the Pho and Cpx single system deletion mutants appear to
458 have similar net contributions to meropenem tolerance both in rate of killing and final
459 viability, while still forming detectable spheroplasts capable of recovery. The versatile
460 PhoPQ system senses Mg^{2+} deficiency, presence of antimicrobial peptides, pH and other
461 stresses [40]. Most relevant to the phenotype assayed here, we have previously shown
462 that PhoPQ is required for meropenem tolerance in the related bacterium *Enterobacter*
463 *cloacae*, via PhoPQ-controlled outer membrane modifications [25]. The Cpx system is a
464 general cell envelope health monitor [41], which controls, among other things, L,D-
465 transpeptidases that help stabilize the outer membrane [42, 43], and respiratory chain
466 functions [44, 45], which contribute to ROS production in spheroplasts [17]. Lastly, the Rcs
467 system contributes to meropenem tolerance in a unique way. Time-dependent killing
468 revealed that viability dropped substantially in the Δ*rcsF* mutant, but this strain's capacity
469 to form spheroplasts and maintain optical density was comparable to the WT parent
470 strain. However, Δ*rcsF* mutant spheroplasts were markedly impaired in their ability to
471 reform successful dividing rods when meropenem is removed. Among other genes, Rcs
472 positively regulates the cell division component *ftsZ* [46], perhaps pointing to a model

473 where upon spheroplast recovery, cell division can commence sooner in WT than in Δ*rcs*
474 cells due to the increased availability of critical divisome components. Taken together,
475 the phenotypes of each individual mutant indicate that aspects of β-lactam tolerance are
476 mediated by distinct response systems, likely with some temporal distinction (**Fig. 8**)

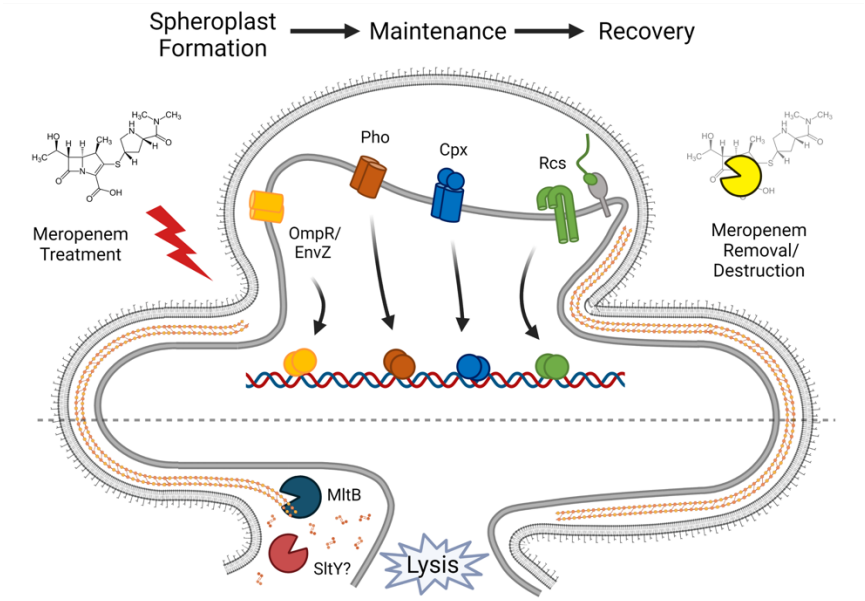

477

478

479 **Figure 8: Summary of meropenem tolerance as a net result of cell wall degradation**
480 **and cell envelope stress response induction** Meropenem treatment induces multiple
481 cell envelope stress responses, whose regulons contribute to survival. Lytic
482 transglycosylases MltB and SltY contribute significantly to sacculus degradation, which
483 reduces efficiency of spheroplast recovery.

484

485 Because TnSeq has the benefit of also revealing gene disruptions that increase
486 fitness, we simultaneously probed for endogenous factors that reduce meropenem
487 tolerance. *K. pneumoniae* strain TS1's lytic transglycosylase *mltB* answered the screen
488 as a strong candidate that actually improves survival when disrupted, which conversely
489 suggests that MltB contributes to cell killing in the presence of meropenem. Lytic

490 transglycosylases cleave glycosidic bonds of peptidoglycan strands [24], and have
491 specific and important functions in opportunistic pathogens. For example, in
492 *Acinetobacter baumannii*, *mltB* is a critical factor for pathogenesis by linking complex
493 envelope homeostasis functions with virulence [47]. In *Pseudomonas aeruginosa*,
494 eliminating this enzyme (also in combination with other lytic transglycosylases) increases
495 resistance to cell-wall targeting antibiotics via induction of an endogenous β-lactamase
496 [48, 49]. Disruption of *sltY* and *mltB* in *K. pneumoniae* strain KPNIH1 resulted in 10- 1000
497 fold increased tolerance to meropenem. Cell morphology around the poles in these
498 mutants was maintained after exposure to meropenem, possibly due to this strain's
499 inability to degrade the old peptidoglycan present when PBPs are inhibited. This
500 maintenance of the cell wall could be what increases survival by preserving the
501 peptidoglycan and envelope-spanning systems, leading to preservation of cell integrity
502 and potentially serving as a scaffold for new cell wall synthesis when meropenem is
503 removed. It is unclear why *mltB* and *sltY* specifically emerge as the only lytic
504 transglycosylases that have this effect on the cell when bacteria generally have multiple
505 redundant lytic transglycosylase paralogs in their genomes; strong phenotypes for single
506 deletion mutants are thus highly unusual. We noted that both LTG mutations also
507 increased meropenem MIC significantly (**Table S2**). It is thus possible that increased
508 degradation of meropenem, for example by overproduction of a chromosomal β-
509 lactamase with low-level carbapenemase activity, also at least partially contributes to
510 enhanced survival of these mutants (as a caveat, *K. pneumoniae'*s chromosomal enzyme
511 SHV-1 is not known to hydrolyze carbapenems). However, these mutants still form
512 spheroplasts, indicating significant cell wall damage, ergo meropenem is still present at

513 supra-MIC concentrations. Putative carbapenemase activity can thus not account entirely
514 for the high survival phenotype.

515 Overall, this study presents a deeper insight into β-lactam tolerance and can inform
516 further investigations to understand other aspects of how these dangerous pathogens
517 respond to antibiotics and ultimately develop resistance. Attaining an understanding of
518 the detailed workings of this complex phenotype can inform approaches toward finding
519 potential druggable targets to reduce or abolish an organism's capacity for β-lactam
520 tolerance, thus allowing development of novel therapeutics and treatment strategies for
521 tolerant pathogens.

522

523 **Methods**

524 *Culture conditions and killing experiments* Unless otherwise stated, all strains were grown
525 in shaking overnight cultures at 37ºC, and tolerance assays were carried out in Brain
526 Heart Infusion (BHI) broth at 37ºC. Tolerance assays were conducted by inoculating
527 overnight culture at a 1:10 ratio into fresh BHI medium containing 10 μg/mL meropenem
528 (TCI, Tokyo, Japan). Cultures were then incubated at 37˚C without shaking. Optical
529 density was measured in a VWR V-1200 spectrophotometer and viable cells were
530 quantified by serial dilution in BHI medium and spot-titered onto BHI agar. The
531 carbapenemase KPC-2 was purified (see next section for detail) and added to culture
532 samples at a final concentration of approximately 1 μg/mL prior to serial dilution to
533 deactivate meropenem, thus eliminating meropenem carryover effect. For

534 complementation experiments, 40 ng/mL anhydrotetracycline was added for induction of
535 expression.

536 *MIC Determination.* MICs for all strain backgrounds (except the isolate panel, see below)
537 were determined by diluting overnight cultures 10^7-fold in BHI medium for direct
538 comparison with killing experiments. Diluted cultures were inoculated into BHI containing
539 successive 2-fold concentrations of meropenem in a 96 well microtiter plate at a final
540 volume of 200 µL per well, and incubated at 37°C overnight, leaving one well as an
541 uninoculated control, and one well with cells but without meropenem to ensure growth of
542 the strain. MICs were recorded as the lowest meropenem concentration free from
543 turbidity. For the clinical isolate panel, MICs were measured using standard CLSI
544 guidelines (cation-adjusted MHB).

545

546 *Purification of* KPC-2 *enzyme*. The gene for KPC-2 was amplified from the genome of
547 *Enterobacter cloacae* strain 41952, a clinical isolate from WCM, and cloned into the
548 pET21 expression vector. The His-tagged KPC-2 enzyme was overexpressed in BL21
549 pLysS. A 500 ml culture of LB containing 100 µg/mL ampicillin was induced at OD=0.5
550 with 1 mM IPTG and incubated shaking at 30°C overnight. The following day, cultures
551 were centrifuged, and pellets were decanted and stored at -80°C until lysis and
552 purification. Pellets were resuspended in resuspension buffer (20 mM Tris, 150 mM NaCl,
553 5 mM imidazole) and sonicated using the QSonica with the largest tip attachment for 40
554 minutes total, alternating between 5 second pulses and 5 second rests on ice. The lysate
555 was then centrifuged for 45 minutes at 16,000 rpm and the supernatant discarded. In
556 preliminary expression experiments, we found that KPC was mostly in the insoluble

557 fraction. The insoluble pellet was resuspended in binding buffer (20 mM Tris, 150 mM
558 NaCl, 5 mM imidazole, 3 M Urea), and incubated rotating overnight at 4°C to denature
559 and solubilize the KPC-2 protein. The next day, the denatured lysate was centrifuged
560 again at 16,000 rpm for 45 minutes, and the resulting supernatant passed through a
561 cobalt-charged NTA agarose resin column at room temperature. Six column volumes of
562 wash buffer (20 mM Tris, 150 mM NaCl, 30 mM imidazole, 3 M Urea) were then passed
563 through the column, and the protein eluted in 1.8 mL fractions with increasing
564 concentrations of imidazole in elution buffers (20 mM Tris, 150 mM NaCl, 50-600 mM
565 imidazole, 3 M Urea). Fractions with the highest protein concentrations were pooled, and
566 the total volume was dialyzed into a final storage buffer (20 mM Tris, 150 mM NaCl, 30%
567 glycerol) in three steps, each with decreasing concentrations of imidazole and increasing
568 concentrations of glycerol. Purity was determined by SDS-PAGE, and concentration was
569 estimated with Bio-Rad Bradford Assay kit.

570

571 *Imaging.* All images were taken on a Leica Mdi8 microscope (Leica Microsystems, GmbH,
572 Wetzlar, Germany) with a PECON TempController 2000-1 (Erbach, Germany), heated
573 stage at 37˚C for growth experiments, or room temperature for static images. For
574 timelapse microscopy of spheroplast formation, cells were placed on a 0.8% agarose pad
575 containing BHI and 10 µg/mL meropenem within a gene frame (ThermoFisher, Waltham,
576 MA). For recovery timelapses, KPC-2 enzyme was added at 5 µg/mL to eliminate the
577 meropenem. Frames were taken using autofocus control every five minutes for up to 12
578 hours. Timelapse video stacks were processed in FIJI (NIH) using the Linear Stack
579 Alignment with SIFT under the Registration plugin (using all default settings with the

580 exception of Expected Transformation, which was changed to Translation) to center cells
581 in the cropped frame. Frame rates were set at 3-4 frames per second for supplemental
582 videos.

583

584 *Transposon mutagenesis screen and data analysis*. *K. pneumoniae* strain TS1 was
585 mutagenized with a Mariner transposon delivered via the *E. coli* donor strain MFD λpir to
586 generate a complex library of kanamycin-resistant transposon mutants. This initial library
587 was frozen as a glycerol stock, and an overnight culture from it was grown in BHI
588 containing kanamycin at 50 µg/mL to form an input library as the comparison for TnSeq
589 analysis. Overnight cultures of this input library were diluted 10-fold into 5 mL BHI
590 containing meropenem (10 ug/mL) and incubated for six hours at 37˚C without shaking,
591 followed by plating on BHI agar plates after treatment with 5 µg/mLKPC-2 enzyme
592 (untreated controls were also generated mirroring the six-hour exposure and recovery
593 populations). Genomic DNA (gDNA) was extracted from all stages of the meropenem
594 challenge and recovery and prepared for Illumina sequencing. Briefly, gDNA extracted
595 from each library was sonicated to generate fragments mostly 200-800 base pairs long
596 which were blunted using NEB Quick Blunting Mix (#E1201L). After blunting, fragments
597 were given A-tails with Taq DNA polymerase to allow ligation of adapter sequences (full
598 lists of primers and reactions can be found in supplemental methods). Ligated fragments
599 were amplified with PCR to enrich transposon-adjacent regions, and then again were
600 PCR amplified with primers to add barcodes, spacer sequences, and Illumina chip
601 attachment ends. The library was run on agarose gel and all fragments 250-600 base
602 pairs were extracted for analysis on the BioAnalyzer (Agilent, Santa Clara, CA) to assess

603 before Illumina sequencing. All libraries were sequenced as paired 150 bp reads, though
604 only forward reads were used in the final analysis.

605 Raw Illumina data were processed in Galaxy using the Cutadapt program to trim
606 reads for length and quality, then mapped with Bowtie2 using the *K. pneumoniae* TS1
607 FASTA reference genome available in NCBI (Biosample accession number
608 SAMN04014921) (full protocol available at this link:
609 https://usegalaxy.org/u/trevorcrossmicro/w/trimming). Mapped reads were analyzed by
610 TnSeq Explorer [50]to calculate insertion density of each gene from each library.
611 Insertion densities were used to calculate an insertion density ratio for each gene from
612 one library to another, thereby comparing essentiality across points in the meropenem
613 challenge. The comparison between library 2 (input) and library 6 (meropenem recovery)
614 was used as the basis for ranking genes in order of essentiality, with genes most essential
615 to meropenem tolerance appearing at the top of the list, while genes which impart a fitness
616 increase when disrupted appearing at the bottom of the list.

617

618 *KPNIH1 validations.* Candidate tolerance genes identified by TnSeq were first validated
619 using an arrayed *K. pneumoniae* KPNIH1 library constructed by the Manoil lab [21].
620 Transposon mutants were grown in 200 µL BHI medium overnight cultures in a 96 well
621 plate. The next day, the overnight culture was diluted 1:10 into BHI containing a final
622 concentration of 10 µg/mL meropenem. At the indicated time points, samples were taken
623 for CFU determination, while simultaneously measuring optical densities in a Spectramax
624 iX3 (Molecular Devices, San Jose, CA) plate reader, and then incubated at 37˚C without
625 shaking for six hours. Final optical density and CFU/mL were recorded and the ratio

626 between final and initial values were calculated to determine the effect of the gene
627 disruption when challenged with meropenem.

628

629 *Strain constructions with pTOX*. Strains and oligos are summarized in Table S5 and S6.
630 Knock out and reporter strains in *K. pneumoniae* TS1 were constructed using the pTOX5
631 allelic exchange vector as described in [51]. Briefly, 800-1000 base pair regions flanking
632 regions were amplified using PCR or synthesized de novo and assembled via isothermal
633 assembly into the pTOX SmaI site. Assembled constructs were transformed into DH5α
634 λpir competent cells, plated on LB containing 100 µg/mL chloramphenicol and 1% glucose
635 (LB/CHL/gluc) (to repress the rhamnose inducible toxin gene) and screened for insertion
636 size with primers TC_82 and TC_83, followed by sequence verification through Sanger
637 sequencing. Correct constructs were transformed into conjugal MFD λpir and mated into
638 *K. pneumoniae* TS1 on LB containing 1% glucose and 1.2 mM DAP (LB/gluc/DAP) for 6
639 hours at 37°C. Transconjugants were isolated back on LB/CHL/gluc and a single colony
640 was grown out in LB containing 1% glucose until the OD reached 0.1-0.2, at which point
641 cells were washed with M9 medium containing 0.2% casamino acids and 1% rhamnose,
642 and plated on solid M9/rham/casamino acids to induce the counterselective toxin and
643 isolate allelic exchange constructs containing the desired modifications. Envelope stress
644 response system deletions were screened using primers flanking the loci of interest and
645 validated using internal primers. Other constructs were validated using primers specific
646 to the modification, or primers flanking the *lac*Z locus where reporters were inserted.

647 For complementation of phenotypes, genes were cloned into a pTn7 plasmid (tn7-
648 gentamycin) and inserted into the chromosomal Tn7 insertion site (near the *glmS* gene)

649 using triparental mating with the helper plasmid pTNS2. The Tn7 plasmid was modified
650 to contain an anydrotetracycline-inducible (Tet on) gene fragment (DL-GB-PP-1, see
651 **Table S6**). MltB and CESRs were amplified from the chromosome of Kp KPNIH1 (*mltB*)
652 and TS1 (CESR loci), respectively, using primers NN520/521 (mltB), NN518/519
653 (*cpxPRA*), NN512/513 (*ompR/envZ*), NN514/515 (*phoPQ*), NN516/517 (*rcsDBC*) and
654 cloned into PacI-digested pTN7 using isothermal assembly. Successful clones were
655 screened for using primers NN522/NN523, and verified via whole plasmid sequencing.

656

657 *Miller assay to detect RcsB function and induction*. To assess function of the RcsB
658 response regulator, a reporter construct was constructed by inserting an *rprA-lacZ*$_{MG1655}$
659 reporter with the *E. coli* MG1655 lacZ gene (abbreviated to *rprA-lacZ*) into the TS1 native
660 *lacZ* locus, eliminating most of the native *lacI* and *lacZ* genes. This construct was
661 validated first by overexpressing native RcsB on a pBAD plasmid in the presence of 0.2%
662 arabinose on BHI medium from strain TS1 in the reporter background and qualitatively
663 comparing X-gal signal to the construct containing an empty vector. RcsB activation upon
664 meropenem exposure was measured by performing the Miller assay on cell pellets from
665 meropenem-exposed cells at 0, 1, 3, and 6 hours in BHI and control cultures to determine
666 relative units of β-galactosidase activity normalized to CFU/mL of either culture.

667

668 **Acknowledgements**

669 This work was supported by NIH grants R01AI143704 and R01GM130971 to TD.
670 AS acknowledges support from NIH-NIGMS via grant R35GM148351.

671 **Supplementary Figures**

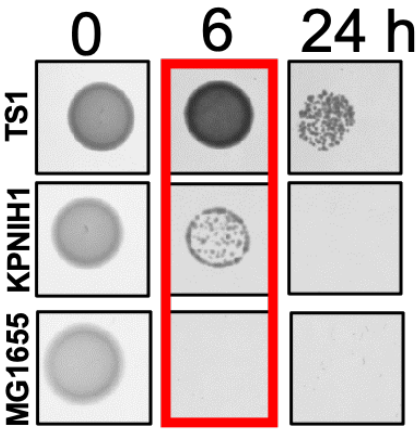

672

673 **Fig. S1 Tolerance screen validation with benchmark isolates.** Strains were exposed
674 to meropenem (10 µg/mL) as described in methods. At the indicated time-points, 10 µL
675 of the cell suspension was spotted on BHI agar and supplemented with KPC, followed by
676 24 hours of incubation at 37 ˚C.

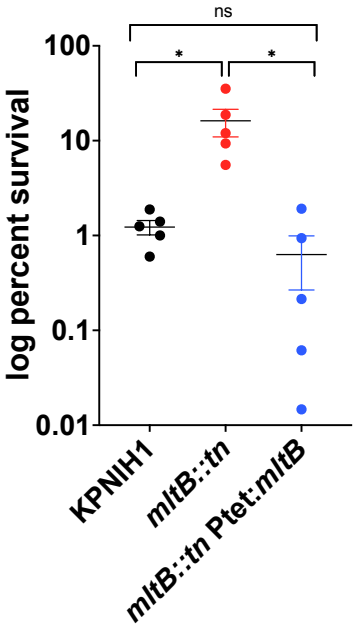

677

678 **Fig. S2 Complementation of the Δ*mltB* phenotype.** The indicated strains were grown
679 overnight in BHI, then diluted 10fold into fresh BHI containing meropenem (10 µg/mL)
680 and 40 ng/mL anhydrotetracycline. Viability was determined by serial dilution and spot-
681 plating after 24 hours of incubation. Shown are raw data points for 5 biological replicates
682 for each strain. Statistical significance was determined by Mann Whitney test (*p < 0.05)

683

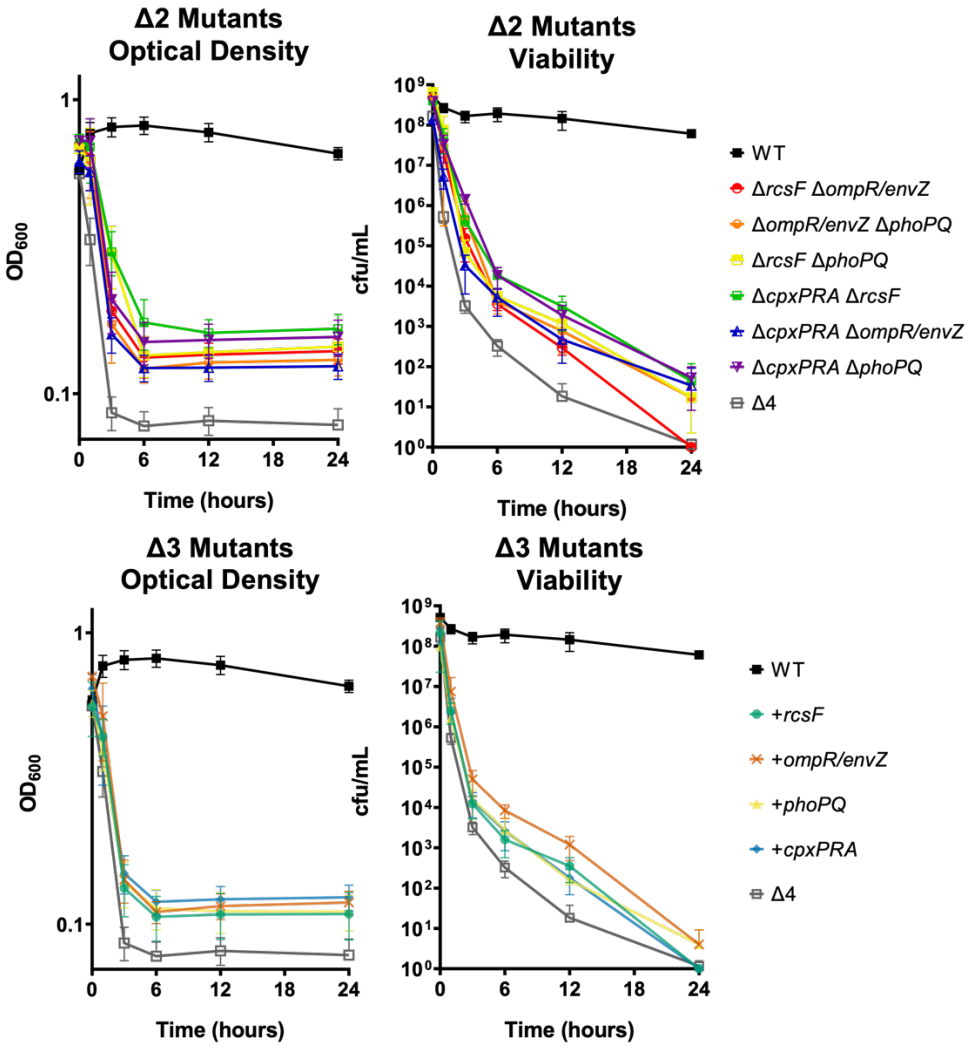

684

685 **Fig. S3 Tolerance phenotypes of CESR mutants.** Time-dependent killing experiments
686 (10 µg/mL meropenem) were conducted in BHI medium. Statistical analysis (Kruskal-

687 Wallace test, $p < 0.001$) revealed statistically significant differences in viability (12 hour
688 time point) for all mutants vs. WT; Δ4 vs. any triple mutant was not statistically significant.

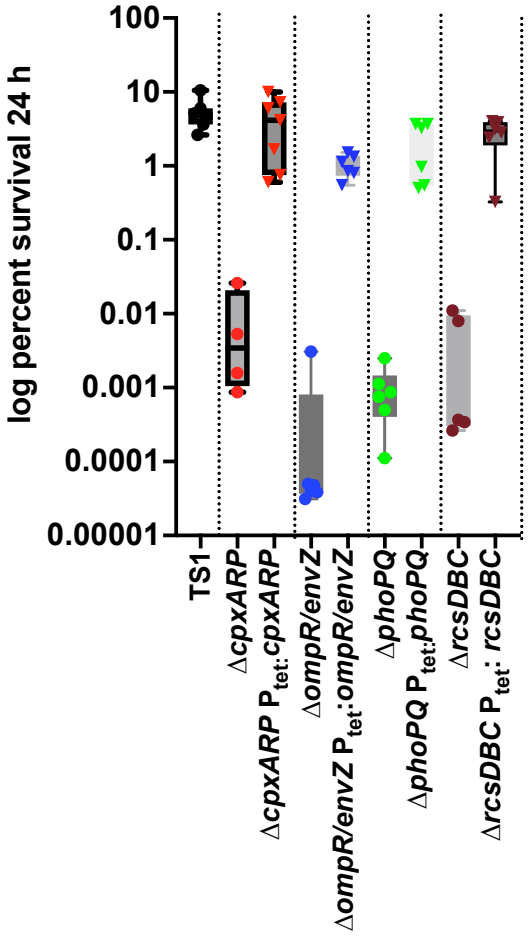

689

690 **Fig. S4 Complementation of the ΔCESR phenotypes.** The indicated strains were
691 grown overnight in BHI, then diluted 10fold into fresh BHI containing meropenem (10
692 µg/mL) and 40 ng/mL anhydrotetracycline and incubated for 24 hours. Viability was
693 determined by serial dilution and spot-plating. Shown are boxplot and raw data points for
694 at least 5 biological replicates for each strain.

695

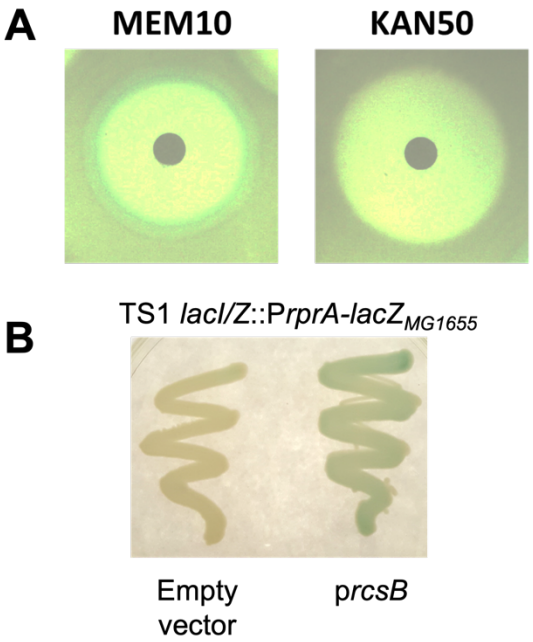

696

697 **Fig. S5 Meropenem induces the Rcs phosphorelay. A)** The P_{rprA}-*lacZ* reporter strain
698 was spread on plates containing the chromogenic LacZ substrate x-gal. A filter disk was
699 placed in the middle containing either meropenem or kanamycin. Note blue halo around
700 the meropenem disk, in the sub-MIC area beyond the zone of inhibition. B) RcsB was
701 overexpressed from an arabinose-inducible promoter in the P_{rprA}-*lacZ* background,
702 followed by plating on LB with X-gal.

703

704 **Supplementary Tables**

705 Table S1 – Bloodstream Isolate Panel Distribution in tolerance categories

706 Table S2 – MICs of the strains used in this study

707 Table S3 – Bloodstream isolate panel

708 Table S4 – TnSeq insertion frequencies

709 Table S5 –Strains used in this study

710 Table S6 – Oligos used in this study

711

712 **References:**

713 1. Miller WR, Arias CA. ESKAPE pathogens: antimicrobial resistance, epidemiology, clinical
714 impact and therapeutics. Nat Rev Microbiol. 2024;22(10):598-616. Epub 2024/06/04. doi:
715 10.1038/s41579-024-01054-w. PubMed PMID: 38831030.
716 2. Haney EF, Hancock REW. Addressing Antibiotic Failure—Beyond Genetically Encoded
717 Antimicrobial Resistance. Frontiers in Drug Discovery. 2022;2. doi: 10.3389/fddsv.2022.892975.
718 3. Balaban NQ, Helaine S, Lewis K, Ackermann M, Aldridge B, Andersson DI, et al.
719 Definitions and guidelines for research on antibiotic persistence. Nat Rev Microbiol.
720 2019;17(7):441-8. Epub 2019/04/14. doi: 10.1038/s41579-019-0196-3. PubMed PMID:
721 30980069; PubMed Central PMCID: PMCPMC7136161.
722 4. Roberts D, Higgs E, Rutman a, Cole P. Isolation of spheroplastic forms of Haemophilus
723 influenzae from sputum in conventionally treated chronic bronchial sepsis using selective medium
724 supplemented with N-acetyl-D-glucosamine: possible reservoir for re-emergence of infection.
725 British medical journal (Clinical research ed). 1984;289:1409-12. doi:
726 10.1016/j.compmedimag.2005.07.001. PubMed PMID: 6437576.
727 5. Monahan LG, Turnbull L, Osvath SR, Birch D, Charles IG, Whitchurch CB. Rapid
728 conversion of Pseudomonas aeruginosa to a spherical cell morphotype facilitates tolerance to
729 carbapenems and penicillins but increases susceptibility to antimicrobial peptides. Antimicrob
730 Agents Chemother. 2014;58(4):1956-62. doi: 10.1128/AAC.01901-13. PubMed PMID: 24419348;
731 PubMed Central PMCID: PMCPMC4023726.
732 6. Dörr T, Davis BM, Waldor MK. Endopeptidase-mediated beta lactam tolerance. PLoS
733 Pathog. 2015;11(4):e1004850. doi: 10.1371/journal.ppat.1004850. PubMed PMID: 25884840;
734 PubMed Central PMCID: PMCPMC4401780.
735 7. Cross T, Ransegnola B, Shin JH, Weaver A, Fauntleroy K, VanNieuwenhze MS, et al.
736 Spheroplast-Mediated Carbapenem Tolerance in Gram-Negative Pathogens. Antimicrob Agents
737 Chemother. 2019;63(9). doi: 10.1128/AAC.00756-19. PubMed PMID: 31285232; PubMed Central
738 PMCID: PMCPMC6709500.
739 8. Mickiewicz KM, Kawai Y, Drage L, Gomes MC, Davison F, Pickard R, et al. Possible role
740 of L-form switching in recurrent urinary tract infection. Nat Commun. 2019;10(1):4379. Epub
741 2019/09/29. doi: 10.1038/s41467-019-12359-3. PubMed PMID: 31558767; PubMed Central
742 PMCID: PMCPMC6763468.
743 9. Claessen D, Errington J. Cell Wall Deficiency as a Coping Strategy for Stress. Trends
744 Microbiol. 2019;27(12):1025-33. Epub 2019/08/20. doi: 10.1016/j.tim.2019.07.008. PubMed
745 PMID: 31420127.
746 10. Errington J. Cell wall-deficient, L-form bacteria in the 21st century: a personal perspective.
747 Biochemical Society Transactions. 2017;45:287-95. doi: 10.1042/BST20160435. PubMed PMID:
748 28408469.
749 11. Paczosa MK, Mecsas J. Klebsiella pneumoniae: Going on the Offense with a Strong
750 Defense. Microbiol Mol Biol Rev. 2016;80(3):629-61. Epub 2016/06/17. doi:

751 10.1128/mmbr.00078-15. PubMed PMID: 27307579; PubMed Central PMCID:
752 PMCPMC4981674.
753 12. Murray CJL, Ikuta KS, Sharara F, Swetschinski L, Robles Aguilar G, Gray A, et al. Global
754 burden of bacterial antimicrobial resistance in 2019: a systematic analysis. The Lancet.
755 2022;399(10325):629-55. doi: 10.1016/S0140-6736(21)02724-0.
756 13. Chen TA, Chuang YT, Lin CH. A Decade-Long Review of the Virulence, Resistance, and
757 Epidemiological Risks of Klebsiella pneumoniae in ICUs. Microorganisms. 2024;12(12). Epub
758 2025/01/08. doi: 10.3390/microorganisms12122548. PubMed PMID: 39770751; PubMed Central
759 PMCID: PMCPMC11678397.
760 14. Dörr T. Understanding tolerance to cell wall–active antibiotics. Annals of the New York
761 Academy of Sciences. 2021;1496(1):35-58. doi: https://doi.org/10.1111/nyas.14541.
762 15. Cho H, Uehara T, Bernhardt TG. Beta-lactam antibiotics induce a lethal malfunctioning of
763 the bacterial cell wall synthesis machinery. Cell. 2014;159(6):1300-11. doi:
764 10.1016/j.cell.2014.11.017. PubMed PMID: 25480295; PubMed Central PMCID:
765 PMCPMC4258230.
766 16. Lobritz MA, Andrews IW, Braff D, Porter CBM, Gutierrez A, Furuta Y, et al. Increased
767 energy demand from anabolic-catabolic processes drives β-lactam antibiotic lethality. Cell Chem
768 Biol. 2022;29(2):276-86.e4. Epub 2022/01/07. doi: 10.1016/j.chembiol.2021.12.010. PubMed
769 PMID: 34990601; PubMed Central PMCID: PMCPMC8857051.
770 17. Shin JH, Choe D, Ransegnola B, Hong HR, Onyekwere I, Cross T, et al. A multifaceted
771 cellular damage repair and prevention pathway promotes high-level tolerance to beta-lactam
772 antibiotics. EMBO Rep. 2021:e51790. Epub 2021/01/20. doi: 10.15252/embr.202051790.
773 PubMed PMID: 33463026.
774 18. Held K, Gasper J, Morgan S, Siehnel R, Singh P, Manoil C. Determinants of Extreme beta-
775 Lactam Tolerance in the Burkholderia pseudomallei Complex. Antimicrob Agents Chemother.
776 2018;62(4). doi: 10.1128/AAC.00068-18. PubMed PMID: 29439964; PubMed Central PMCID:
777 PMCPMC5913950.
778 19. Dörr T, Alvarez L, Delgado F, Davis BM, Cava F, Waldor MK. A cell wall damage response
779 mediated by a sensor kinase/response regulator pair enables beta-lactam tolerance. Proc Natl
780 Acad Sci U S A. 2016;113(2):404-9. doi: 10.1073/pnas.1520333113. PubMed PMID: 26712007;
781 PubMed Central PMCID: PMCPMC4720315.
782 20. Gefen O, Chekol B, Strahilevitz J, Balaban NQ. TDtest: easy detection of bacterial
783 tolerance and persistence in clinical isolates by a modified disk-diffusion assay. Sci Rep.
784 2017;7:41284. doi: 10.1038/srep41284. PubMed PMID: 28145464; PubMed Central PMCID:
785 PMCPMC5286521 financial interests in this work.
786 21. Ramage B, Erolin R, Held K, Gasper J, Weiss E, Brittnacher M, et al. Comprehensive
787 Arrayed Transposon Mutant Library of Klebsiella pneumoniae Outbreak Strain KPNIH1. J
788 Bacteriol. 2017;199(20). doi: 10.1128/JB.00352-17. PubMed PMID: 28760848; PubMed Central
789 PMCID: PMCPMC5637181.
790 22. Weaver AI, Murphy SG, Umans B, Tallavajhala S, Onyekwere I, Wittels S, et al. Genetic
791 determinants of penicillin tolerance in Vibrio cholerae. Antimicrob Agents Chemother. 2018. doi:
792 10.1128/AAC.01326-18. PubMed PMID: 30061291.
793 23. Ranjit DK, Jorgenson MA, Young KD. PBP1B Glycosyltransferase and Transpeptidase
794 Activities Play Different Essential Roles during the De Novo Regeneration of Rod Morphology in
795 Escherichia coli. J Bacteriol. 2017;199(7). Epub 2017/01/18. doi: 10.1128/jb.00612-16. PubMed
796 PMID: 28096447; PubMed Central PMCID: PMCPMC5350282.
797 24. Weaver A, Taguchi A, Dörr T. Masters of Misdirection: Peptidoglycan Glycosidases in
798 Bacterial Growth. J Bacteriol. 2023;205(3):e0042822. Epub 2023/02/10. doi: 10.1128/jb.00428-
799 22. PubMed PMID: 36757204; PubMed Central PMCID: PMCPMC10029718.
800 25. Murtha AN, Kazi MI, Schargel RD, Cross T, Fihn C, Cattoir V, et al. High-level carbapenem
801 tolerance requires antibiotic-induced outer membrane modifications. PLoS Pathog.

2022;18(2):e1010307. Epub 20220207. doi: 10.1371/journal.ppat.1010307. PubMed PMID: 35130322; PubMed Central PMCID: PMCPMC8853513.
26. Ranjit DK, Young KD. The Rcs stress response and accessory envelope proteins are required for de novo generation of cell shape in Escherichia coli. J Bacteriol. 2013;195(11):2452-62. Epub 2013/04/02. doi: 10.1128/JB.00160-13. PubMed PMID: 23543719; PubMed Central PMCID: PMCPMC3676047.
27. Laubacher ME, Ades SE. The Rcs phosphorelay is a cell envelope stress response activated by peptidoglycan stress and contributes to intrinsic antibiotic resistance. J Bacteriol. 2008;190(6):2065-74. doi: 10.1128/JB.01740-07. PubMed PMID: 18192383; PubMed Central PMCID: PMCPMC2258881.
28. Rousseau CJ, Fraikin N, Zedek S, Van Melderen L. Are envelope stress responses essential for persistence to β-lactams in Escherichia coli? Antimicrob Agents Chemother. 2023;67(10):e0032923. Epub 2023/10/03. doi: 10.1128/aac.00329-23. PubMed PMID: 37787525; PubMed Central PMCID: PMCPMC10583663.
29. Wall E, Majdalani N, Gottesman S. The Complex Rcs Regulatory Cascade. Annu Rev Microbiol. 2018;72:111-39. doi: 10.1146/annurev-micro-090817-062640. PubMed PMID: 29897834.
30. Harmange G, Hueros RAR, Schaff DL, Emert B, Saint-Antoine M, Kim LC, et al. Disrupting cellular memory to overcome drug resistance. Nature Communications. 2023;14(1):7130. doi: 10.1038/s41467-023-41811-8.
31. Shaffer SM, Dunagin MC, Torborg SR, Torre EA, Emert B, Krepler C, et al. Rare cell variability and drug-induced reprogramming as a mode of cancer drug resistance. Nature. 2017;546(7658):431-5. doi: 10.1038/nature22794.
32. Singh A, Saint-Antoine M. Probing transient memory of cellular states using single-cell lineages. Frontiers in Microbiology. 2023;13. doi: 10.3389/fmicb.2022.1050516.
33. Hossain T, Singh A, Butzin NC. Escherichia coli cells are primed for survival before lethal antibiotic stress. Microbiology Spectrum. 2023;11(5):e01219-23. doi: doi:10.1128/spectrum.01219-23.
34. Guha M, Singh A, Butzin NC. Priestia megaterium cells are primed for surviving lethal doses of antibiotics and chemical stress. Communications Biology. 2025;8(1):206. doi: 10.1038/s42003-025-07639-2.
35. Lee JJ, Swanson DH, Lee S-K, Dihardjo S, Lee GY, Gelle S, et al. Trehalose catalytic shift inherently enhances phenotypic heterogeneity and multidrug resistance in Mycobacterium tuberculosis. Nature Communications. 2025;16(1):6442. doi: 10.1038/s41467-025-61703-3.
36. Krishnamoorthy K, Lee M. Improved tests for the equality of normal coefficients of variation. Computational Statistics. 2014;29(1):215-32. doi: 10.1007/s00180-013-0445-2.
37. Recacha E, Fox V, Díaz-Díaz S, García-Duque A, Docobo-Pérez F, Pascual Á, et al. Disbalancing Envelope Stress Responses as a Strategy for Sensitization of Escherichia coli to Antimicrobial Agents. Frontiers in Microbiology. 2021;Volume 12 - 2021. doi: 10.3389/fmicb.2021.653479.
38. Rome K, Borde C, Taher R, Cayron J, Lesterlin C, Gueguen E, et al. The Two-Component System ZraPSR Is a Novel ESR that Contributes to Intrinsic Antibiotic Tolerance in Escherichia coli. Journal of Molecular Biology. 2018;430(24):4971-85. doi: https://doi.org/10.1016/j.jmb.2018.10.021.
39. Kenney LJ, Anand GS. EnvZ/OmpR Two-Component Signaling: An Archetype System That Can Function Noncanonically. EcoSal Plus. 2020;9(1). Epub 2020/02/01. doi: 10.1128/ecosalplus.ESP-0001-2019. PubMed PMID: 32003321; PubMed Central PMCID: PMCPMC7192543.
40. Groisman EA, Duprey A, Choi J. How the PhoP/PhoQ System Controls Virulence and Mg(2+) Homeostasis: Lessons in Signal Transduction, Pathogenesis, Physiology, and Evolution.

852 Microbiol Mol Biol Rev. 2021;85(3):e0017620. Epub 2021/07/01. doi: 10.1128/mmbr.00176-20.
853 PubMed PMID: 34191587; PubMed Central PMCID: PMCPMC8483708.
854 41. Raivio TL. Everything old is new again: an update on current research on the Cpx
855 envelope stress response. Biochim Biophys Acta. 2014;1843(8):1529-41. Epub 2013/11/05. doi:
856 10.1016/j.bbamcr.2013.10.018. PubMed PMID: 24184210.
857 42. Morè N, Martorana AM, Biboy J, Otten C, Winkle M, Serrano CKG, et al. Peptidoglycan
858 Remodeling Enables Escherichia coli To Survive Severe Outer Membrane Assembly Defect.
859 mBio. 2019;10(1). Epub 2019/02/07. doi: 10.1128/mBio.02729-18. PubMed PMID: 30723128;
860 PubMed Central PMCID: PMCPMC6428754.
861 43. Bernal-Cabas M, Ayala JA, Raivio TL. The Cpx envelope stress response modifies
862 peptidoglycan cross-linking via the L,D-transpeptidase LdtD and the novel protein YgaU. J
863 Bacteriol. 2015;197(3):603-14. Epub 2014/11/26. doi: 10.1128/jb.02449-14. PubMed PMID:
864 25422305; PubMed Central PMCID: PMCPMC4285979.
865 44. Guest RL, Wang J, Wong JL, Raivio TL. A Bacterial Stress Response Regulates
866 Respiratory Protein Complexes To Control Envelope Stress Adaptation. J Bacteriol.
867 2017;199(20). Epub 2017/08/02. doi: 10.1128/jb.00153-17. PubMed PMID: 28760851; PubMed
868 Central PMCID: PMCPMC5637174.
869 45. Tsviklist V, Guest RL, Raivio TL. The Cpx Stress Response Regulates Turnover of
870 Respiratory Chain Proteins at the Inner Membrane of Escherichia coli. Front Microbiol.
871 2021;12:732288. Epub 2022/02/15. doi: 10.3389/fmicb.2021.732288. PubMed PMID: 35154019;
872 PubMed Central PMCID: PMCPMC8831704.
873 46. Carballès F, Bertrand C, Bouché JP, Cam K. Regulation of Escherichia coli cell division
874 genes ftsA and ftsZ by the two-component system rcsC-rcsB. Mol Microbiol. 1999;34(3):442-50.
875 Epub 1999/11/17. doi: 10.1046/j.1365-2958.1999.01605.x. PubMed PMID: 10564486.
876 47. Crépin S, Ottosen EN, Peters K, Smith SN, Himpsl SD, Vollmer W, et al. The lytic
877 transglycosylase MltB connects membrane homeostasis and in vivo fitness of Acinetobacter
878 baumannii. Mol Microbiol. 2018;109(6):745-62. Epub 2018/06/10. doi: 10.1111/mmi.14000.
879 PubMed PMID: 29884996; PubMed Central PMCID: PMCPMC6185781.
880 48. Cavallari JF, Lamers RP, Scheurwater EM, Matos AL, Burrows LL. Changes to its
881 peptidoglycan-remodeling enzyme repertoire modulate β-lactam resistance in Pseudomonas
882 aeruginosa. Antimicrob Agents Chemother. 2013;57(7):3078-84. Epub 2013/04/25. doi:
883 10.1128/aac.00268-13. PubMed PMID: 23612194; PubMed Central PMCID: PMCPMC3697359.
884 49. Lamers RP, Nguyen UT, Nguyen Y, Buensuceso RN, Burrows LL. Loss of membrane-
885 bound lytic transglycosylases increases outer membrane permeability and β-lactam sensitivity in
886 Pseudomonas aeruginosa. Microbiologyopen. 2015;4(6):879-95. Epub 2015/09/17. doi:
887 10.1002/mbo3.286. PubMed PMID: 26374494; PubMed Central PMCID: PMCPMC4694138.
888 50. Solaimanpour S, Sarmiento F, Mrázek J. Tn-Seq Explorer: A Tool for Analysis of High-
889 Throughput Sequencing Data of Transposon Mutant Libraries. PLOS ONE.
890 2015;10(5):e0126070. doi: 10.1371/journal.pone.0126070.
891 51. Lazarus JE, Warr AR, Kuehl CJ, Giorgio RT, Davis BM, Waldor MK. A New Suite of Allelic-
892 Exchange Vectors for the Scarless Modification of Proteobacterial Genomes. Appl Environ
893 Microbiol. 2019;85(16). Epub 2019/06/16. doi: 10.1128/aem.00990-19. PubMed PMID:
894 31201277; PubMed Central PMCID: PMCPMC6677854.

895